7212–7225 Nucleic Acids Research, 2017, Vol. 45, No. 12
doi: 10.1093/nar/gkx340
Published online 8 May 2017

A non-canonical site reveals the cooperative mechanisms of microRNA-mediated silencing

Mathieu N. Flamand[1], Hin Hark Gan[2], Vinay K. Mayya[1], Kristin C. Gunsalus[2,3] and Thomas F. Duchaine[1,*]

[1]Department of Biochemistry & Goodman Cancer Research Centre, McGill University, Montreal, Quebec H3G 1Y6 Canada, [2]Center for Genomics and Systems Biology, Department of Biology, New York University, 12 Waverly Place, New York, NY 10003, USA and [3]Division of Biology, New York University Abu Dhabi, Abu Dhabi, UAE

Received February 28, 2017; Revised April 05, 2017; Editorial Decision April 17, 2017; Accepted April 18, 2017

ABSTRACT

Although strong evidence supports the importance of their cooperative interactions, microRNA (miRNA)-binding sites are still largely investigated as functionally independent regulatory units. Here, a survey of alternative 3′UTR isoforms implicates a non-canonical seedless site in cooperative miRNA-mediated silencing. While required for target mRNA deadenylation and silencing, this site is not sufficient on its own to physically recruit miRISC. Instead, it relies on facilitating interactions with a nearby canonical seed-pairing site to recruit the Argonaute complexes. We further show that cooperation between miRNA target sites is necessary for silencing *in vivo* in the *C. elegans* embryo, and for the recruitment of the Ccr4-Not effector complex. Using a structural model of cooperating miRISCs, we identified allosteric determinants of cooperative miRNA-mediated silencing that are required for both embryonic and larval miRNA functions. Our results delineate multiple cooperative mechanisms in miRNA-mediated silencing and further support the consideration of target site cooperation as a fundamental characteristic of miRNA function.

INTRODUCTION

The short, non-coding microRNAs (miRNAs) regulate gene expression by base pairing with the 3′ untranslated regions (3′UTRs) of cognate mRNAs and impinging on their translation and stability (1–3). miRNAs are matured from gene-encoded RNA hairpins, are loaded into Argonaute proteins, and then direct effector activities associated with the miRNA-Induced Silencing Complex (miRISC) (4). For the majority of known miRNA targets in animals, miRNAs hybridize imperfectly to mRNAs, leaving bulges in the heteroduplex. Incomplete base pairing at positions 10–11 of the miRNA prevents the slicing activity of the PIWI domain of Argonautes and instead directs partial translational repression, followed by mRNA deadenylation and de-stabilization (2,5,6). Studies conducted in various species indicate that those effector mechanisms are largely instigated through the activities of the Ccr4–Not deadenylase complex and the co-factors it recruits (7–12).

The biological function of a miRNA is defined by the identity of its target(s) and the extent of their induced silencing. Because of the partial nature of base pairing between miRNAs and their mRNA targets in metazoans, the systematic identification of target mRNAs remains a challenge, which still can only be fully answered through direct functional validation. Canonical mRNA-miRNA interactions occur through the 5′ region of the miRNA (nucleotides 2–7), a sequence called the seed that is a pervasive determinant in the recognition of target sites in mRNAs (13). While the quality of seed pairing is one of the most commonly used predictors of silencing output on targets, biologically important sites that do not respect canonical seed base pairing have been discovered for a number of targets (14–17). Several alternative modes of target recognition by miRISC have recently been identified, including pivot seed pairing or nucleation bulge (18), center-pairing miRNA-binding sites (19), or other less-well defined modes of base pairing (20). Other mRNA determinants also have an important contribution in target recognition and potentiation of silencing. For example, miRNA binding sites in proximity to the poly(A) tail or the stop codon of the mRNA target are more likely to have a greater impact on silencing (21).

Several studies have supported the cooperative nature of miRNA-binding sites in silencing. Early genome-wide studies indicated that miRNA-binding sites located in neighboring sequences are more likely to drive silencing than sites separated by more than 50 nucleotides in a 3′UTR (21,22). Fully base-paired or bulged seed-pairing sites cooperatively recruit Ago1, Ago3 and Ago4 in mammalian cells (23). Our own findings indicate that at least two miRNA-binding sites are required to trigger the deadenylation of reporters in a *C.*

*To whom correspondence should be addressed. Tel: +1 514 398 0639; Fax: +1 514 398 6769; Email: thomas.duchaine@mcgill.ca

elegans cell-free embryonic system, and juxtaposition of additional sites greatly potentiates this activity (24). In spite of this evidence, miRNA-binding sites are still overwhelmingly validated and studied as separate, independent regulatory units.

Two distinct mechanisms of miRNA cooperation have been proposed (23): cooperativity in binding, and cooperativity in silencing. Binding cooperativity entails the recruitment of a first miRISC complex to a 3′UTR that enhances the recruitment of subsequent miRISC units to one or multiple distinct target site(s) through physical miRISC–miRISC interactions. However, the determinants for such interactions are unknown, and how they lead to the potentiation of miRNA-binding site silencing remains unclear. Here, we uncover the properties of a non-canonical miRNA-binding site that reveal multiple, distinct mechanisms of miRNA cooperation. An *in vivo* survey of modeled cooperative Argonaute–Argonaute interaction interfaces implicates allosteric determinants in the potentiation of miRNA-mediated silencing.

MATERIALS AND METHODS

C. elegans methods

C. elegans strains were grown in standard conditions (25). For the 2′-*O*-Me pulldown experiments, embryos were obtained by hypochlorite treatment of gravid adult animals. For double site pulldowns (2′-*O*-Me miRISC capture), early embryonic preparations were allowed to develop 4–6 h post-hypochlorite in M9 buffer to favor later stage embryos and increase Bantam expression. Strains were generally maintained at 16°C, unless specified.

Genome Editing

Genome editing for the *alg-1* variants was done as in (26). For 3xFLAG tags insertion and miR-35 binding sites insertion, the genome editing protocol was modified from (27). mRNP complex was assembled with rCAS9 and *in vitro* transcribed modified sgRNA(F+E) (26). Injection mixes contained 1.2 μg/μl CAS9, 300 mM KCl, 12.5 mM Hepes pH 7.4. 50 ng/μl dpy-10 sgRNA, 200 ng/μl gene specific sgRNA, 13.75 ng/μl dpy-10 repair ssODN and 110 ng/μl of gene specific ssODN. Approximately 40 germlines of N2 feed with ds-*cku80* expressing HT115 were injected for each edition.

Preparation of embryonic extracts, and *in vitro* translation assays were conducted as in (28).

***In vitro* transcription, mRNA stability, deadenylation assays and mRNA target cloning** performed as described in (24). Half-deadenylation times were calculated by determining the intersect of the non-deadenylated and deadenylated RNA species over time using polynomial regression (order 2) (R Project), using quantification of autoradiographs with ImageJ. DRIP was performed in triplicates as in (29), except that anti-FLAG antibody was used for immunoprecipitation instead of anti-GFP. Bound RNA was extracted from the beads using 1 ml of QIAZOL reagent according to the manufacturer's instruction and resuspended in 50 uL H_2O. 10% of the RNA was immediately reverse-transcribed using GoScript reverse transcriptase (Promega), with 2 mM $MgCl_2$ and 0.2 μM of gene specific primer for 5 min at 25°C, 1 h at 42°C and inactivated at 75°C for 15 min. The cDNA was diluted 10-fold in H_2O and qPCR was performed conditions and primers described in Supplementary Materials and Methods.

2′-O-Methyl (2′-O-Me) pulldown. N2 embryos were homogenized in 2 volume of lysis buffer (25 mM Hepes–KOH pH 7.4, 150 mM NaCl, 1 mM EDTA, 1 mM DTT, 10% glycerol, 0.5% Triton X-100 and protease inhibitors) using 30 strokes from a stainless steel homogenizer. 20 μl T1 streptadividin beads were pre-incubated with biotinylated 2′-*O*-Me oligonucleotides (10 pmol) for 15 min at 22°C in B&E buffer according to manufacturer's instruction. Extract was spun at max speed for 10 min in a tabletop centrifuge at 4°C three times. Supernatant was incubated with the streptavidin beads for 30 min at 22°C. Beads were washed three times using ice-cold lysis buffer containing 0.1% Triton X-100 and 2 mM DTT, followed by a wash without detergent and 2 mM DTT. Beads were resuspended in 1 volume of 2× SDS loading buffer and eluted by heating at 95°C for 3 min. At least one fifth of the proteins is loaded on gel and analyzed by western blot.

Western blotting. Antibodies used during this study were: rabbit polyclonals against ALG-1/2, ALG-1, DCR-1, AIN-1 and; mouse monoclonal against GFP (Roche), Tubulin and M2 anti-FLAG (Sigma). Goat HRP-conjugated anti-rabbit and anti-mouse were used as secondary antibodies. For quantitative western blots, proteins were transferred to Immobilon-FL, blocked and blotted in Odyssey blocking buffer (PBS) (LI-COR). The proteins were detected with either IRDye© 800CW Goat anti-rabbit IgG or IRDye© 680RD Goat anti-mouse antibodies according to the manufacturer's instructions.

Modeling of the miRISC–miRISC complex

We modeled cooperative complexes starting from *C. elegans* Argonaute sequences and secondary miRNA–target duplexes. Our model construction is based on the algorithm we developed previously to construct miRISC structures (30) and a method for merging miRISCs. Briefly, to construct miRISC structures, we generated up to 1000 3D duplex conformations for each miRNA–target duplex using the MC-Sym algorithm (31), used the Modeller software to produce homology models for *ce*ALG-1 and *ce*ALG-2, sampled open Ago conformations using an elastic network model theory, docked each duplex conformation to each open Ago conformation, and screened for favorable miRISC structures with minimal steric clashes, followed by structure refinement using energy minimization. For *ce*ALG-1/2 modeling, we used both *hs*AGO1 and *hs*AGO2 crystal structures. *ce*ALG-1/2 and *hs*AGO1/2 share ∼67% sequence identity, which exceeds the 50% sequence identity threshold for Modeller to generate reliable homology models. Superimposed structures of *hs*Ago1/ALG-1 and *hs*Ago2/ALG-2 have RMSD values of 3.0 and 1.5 Å, respectively. In subsequent analysis, we chose the more accurate ALG-2 model for building cooperative complexes. Next, the two bound

miRISC units were merged by modeling the possible conformations of CUU linkers connecting the two miRNA target sites, based on ∼2000 observed single-stranded CUU fragments in the PDB database. We selected and energy minimized conformations of the merged miRISCs with the fewest steric clashes. This miRISC merging method predicted a cluster of closely related miRISC–miRISC conformations, which were used in subsequent analysis.

Computational screening of point mutations at the cooperative interface

For mutational analysis, we used the predicted miRISC–miRISC conformations to define four five interacting residues (C_α–C_α distance: <7 Å) between adjacent ALG-2 structures. The interacting residues in ALG-2 are: Arg471, Arg487, Gln730 and Gln748. In ALG-1 the homologous residues are Arg566, Arg581, Gln824, and Gln842. We performed exhaustive point mutations for each residue using pymol's mutagenesis function for a total of 95 mutant complexes. The mutant complexes were then energy minimized and their binding free energies computed using a method we described previously (32). Selection of candidate complexes for experimental verification was based on the magnitude of change in binding energy ($\Delta\Delta G$) and residue conservation.

RESULTS

Alternative 3′UTRs reveal a functional non-canonical miRNA-binding site

Several of the miR-35-42 and *C. elegans* Bantam (miR-58, miR-80-82) miRNA target genes identified in a previous cell-free functional survey (24) encode multiple 3′UTR isoforms. This diversity was also reflected by recent transcriptome-wide 3′UTR capture analyses (33,34). One of those targets, *toh-1*, is expressed as four distinct 3′UTR isoforms, produced by alternative polyadenylation (APA) sites (Figure 1A). Strikingly, in each case the APA site maps within five nucleotides upstream of the seed-complementary sequences of predicted and confirmed miRNA-binding sites (Supplementary Figure S1). We took advantage of the diversity of *toh-1* 3′UTRs to examine the impact of APA on the function of the miRNA-binding sites. Individual 3′UTR isoforms were fused to the *Renilla* luciferase (RL) open reading frame (ORF) and analysed for miRNA-mediated deadenylation and translational repression using a cell-free extract derived from *C. elegans* embryos. Consistent with previous data, full-length (FL) *toh-1* 3′UTR directed rapid deadenylation (time of half-deadenylation ($T_{1/2d}$) 40.2 ± 1.4 min, Figure 1B and C). This 3′UTR encodes cooperating sites for the Bantam and miR-35-42 families in its 5′ most portion. The m232 and m86 3′UTR isoforms are predicted to maintain the cooperative interaction between miR-35-42 and Bantam families, and were efficiently deadenylated ($T_{1/2d}$ 42.4 ± 2.3 min and 34.7 ± 1.4 min, respectively; Figure 1C). Interestingly, the m232 3′UTR is deadenylated slightly faster than the FL 3′UTR. This indicates that while shortening of 3′UTRs can lead to loss of miRNA-binding sites, it can also potentiate the deadenylase output driven by sites advantageously relocated near the poly(A) tail.

Algorithm prediction with a strong weight on the seed contribution identified a single miRNA-binding site (targeted by Bantam) in the shortest isoform of *toh-1* (m35; Figures 1A). Such an extreme shortening of the 3′UTR by APA would be expected to break cooperative interactions between the Bantam and miR-35-42 binding sites. However, the m35 3′UTR still directed deadenylation, albeit at a slower pace in comparison with the other isoforms ($T_{1/2d}$ 122 ± 9 min, Figure 1C and D). Deadenylation of this isoform was unexpected, as a single miRNA-binding site is insufficient to trigger deadenylation or silencing of reporters in this system (24). Deadenylation and translational repression of a RL-*toh-1*-m35 reporter was still dependent on Bantam recognition, as it was inhibited by anti-miR-58 2′-*O*-methylated (2′-*O*-Me) oligonucleotides (35) and remained unaffected by non-specific anti-miR-1, anti-miR-52 or anti-miR-87 2′-*O*-Me oligonucleotides (Figure 1D, and data not shown). No miRNA-binding site matching known seed sequences could be identified, even when allowing for G:U wobble base-paring.

Surprisingly, both deadenylation and translational repression of the m35 3′UTR were specifically prevented by an anti-miR-35 2′-*O*-Me (Figure 1D, and Supplementary Figure S1). We thus hypothesized that seed-oriented prediction may have missed non-canonical miRNA-binding site(s) that contribute to the deadenylation of the m35 3′UTR isoform. Upon examination with the RNAhybrid prediction algorithm (36), three candidate seedless base pairing sites for the miR-35-42 miRNA family were identified (ss1, ss2, ss3). The candidate sites were predicted to base-pair with ΔG_{min} of –18.7 kcal/mol (ss1), –23.2 kcal/mol (ss2) and –16.2 kcal/mol (ss3) (Figure 1E). We mutated each of these candidate sites (mutations introduced are indicated in red in Figure 1E and Supplementary Figure S1) and tested the mutant 3′UTRs in deadenylation assays. Mutation of ss3 prevented m35 deadenylation, while mutation of ss1 and ss2 had no detectable effect (Figure 1F, Supplementary Figure S1). Thus, both the seed-pairing Bantam and the seedless ss3 sites are required to direct miRNA-mediated deadenylation of the *toh-1* m35 3′UTR. However, neither alone is sufficient to enable deadenylation. Taken together, these results suggest that seedless miRNA-binding sites can cooperate with seed-pairing sites to trigger miRNA-mediated deadenylation and translation repression.

The ss3 seedless site features unpaired nucleotides in the seed-complementary region at positions 2 and 5 of miR-35, the best-matching miRNA of the miR-35-42 family. It bears a central bulge at positions 9 and 10 and extensive 3′ base pairing with a single bulge in the 3′ half of the site at position 16. Additionally, ss3 presents three possible G:U wobble pairs at positions 11, 18 and 21 of the miRNA (Figure 2A). Moreover, the 5′-most portion is well conserved across close nematodes species (Supplementary Figure S1). This conformation is not compatible with recently described centre-paired sites (19) or with the pivot seed conformation (18). We mutated each base-paired region of ss3 and tested the resulting 3′UTRs in deadenylation assays (Figure 2B). Mutation of any of the regions—5′ (seed-pairing), Mid (matching nts 11–15), and 3′ (nts 17–21)—effectively prevented target deadenylation, indicating strict base pairing and/or struc-

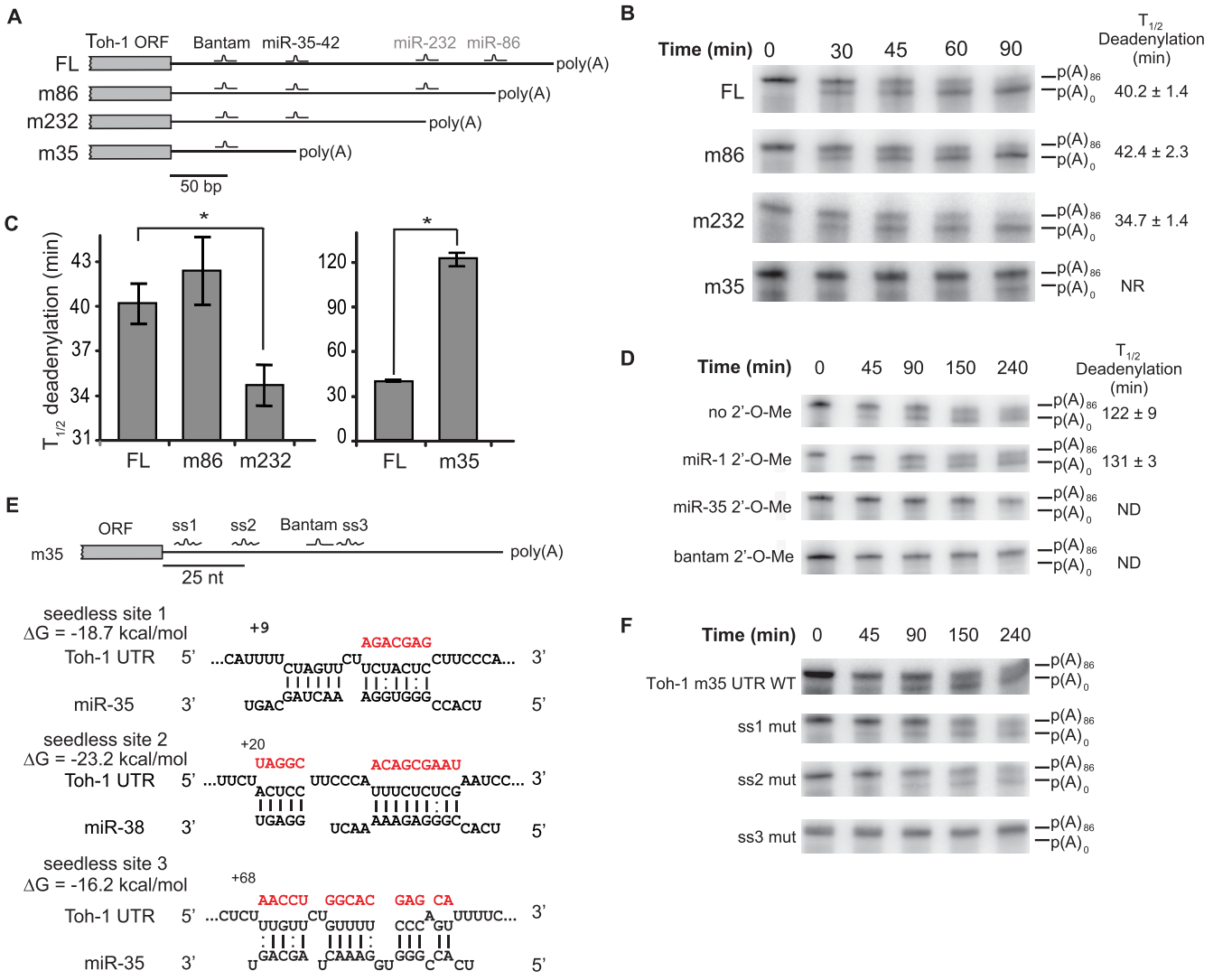

Figure 1. Differential regulation of *toh-1* 3′UTR isoforms by miRNAs. (**A**) 3′RACE of *toh-1* mRNA. 3′UTRs are depicted with seed-pairing binding sites for embryonically expressed miRNAs. Sites contributing or non-contributing to silencing in embryonic cell-free assays are labeled in black and grey, respectively. 3′UTR isoforms are named after the closest miRNA-binding site deleted by alternative polyadenylation sites (APA; FL, m86, m232, m35). (**B**) *In vitro* deadenylation time-courses of alternative 3′UTRs. Half-completion deadenylation times ($T_{1/2d}$) are indicated on the right. (**C**) Quantification of time-courses presented in (B and D) showing potentiation (m232) and delay (m35) of miRNA-mediated deadenylation in comparison to the longer (FL) isoform. Note the different y-axis scale. Data is based on three independent technical replicates. Error bars represent SD. Asterisk indicates a *P*-value of <0.05 in Welch's *T* test. (**D**) Screen for embryonic miRNA families driving m35 3′UTR deadenylation. Experiments carried out using 2′-*O*-Me oligonucleotide inhibitors, fully complementary to miR-1 (negative control), miR-81 (a Bantam family member) and miR-35 are presented. Half-completion deadenylation times ($T_{1/2d}$) are indicated on the right. (**E**) Three candidate seedless miRNA-binding sites for the miR-35–42 family identified using RNAhybrid. Best predicted base pairing of *toh-1* m35 3′UTR with a miR-35–42 family member is represented, as well as their predicted minimum free energy (ΔG). Watson–Crick, and G:U wobble base-pairs are indicated. Position of the 3′-most base-paired nucleotide is indicated relative to the stop codon. (**F**) A seedless miRNA-binding site is functional in the m35 3′UTR. Each candidate seedless site identified in (E) was mutated and subjected to a deadenylation time-course. Mutated sequences for each candidate site are indicated in red in (E). Note the close proximity of the ss3 seedless site with the Bantam-binding site. ND: no deadenylation detected. NR: half-deadenylation was not reached in the time-course. See also Supplementary Figure S1.

tural requirements. Strikingly, the 3′-most base-paired nucleotide of ss3 is located only 1 nucleotide away from the first nucleotide matching the seed region of Bantam. Increasing the distance between the two sites by a few nucleotides substantially slowed deadenylation (Figure 2C). $T_{1/2d}$ increased from 169 min to 264 and 399 min when two or six nucleotides were introduced between the sites, respectively (Figure 2C). This result indicates that the cooperative interaction between the Bantam and ss3 sites is extremely sensitive to the spacing of the sites. Furthermore, restoring the seed-pairing nucleotides of ss3 (nucleotides 2 and 5) resulted in potent acceleration of reporter deadenylation (Figure 2D, seed restore panel). In contrast with the ss3 base-pairing requirements, un-pairing the 3′-most nucleotides of the miR-35-binding site in the seed-restored cooperative pair significantly accelerated deadenylation (Figure 2D, *seed restore* + 3′mut).

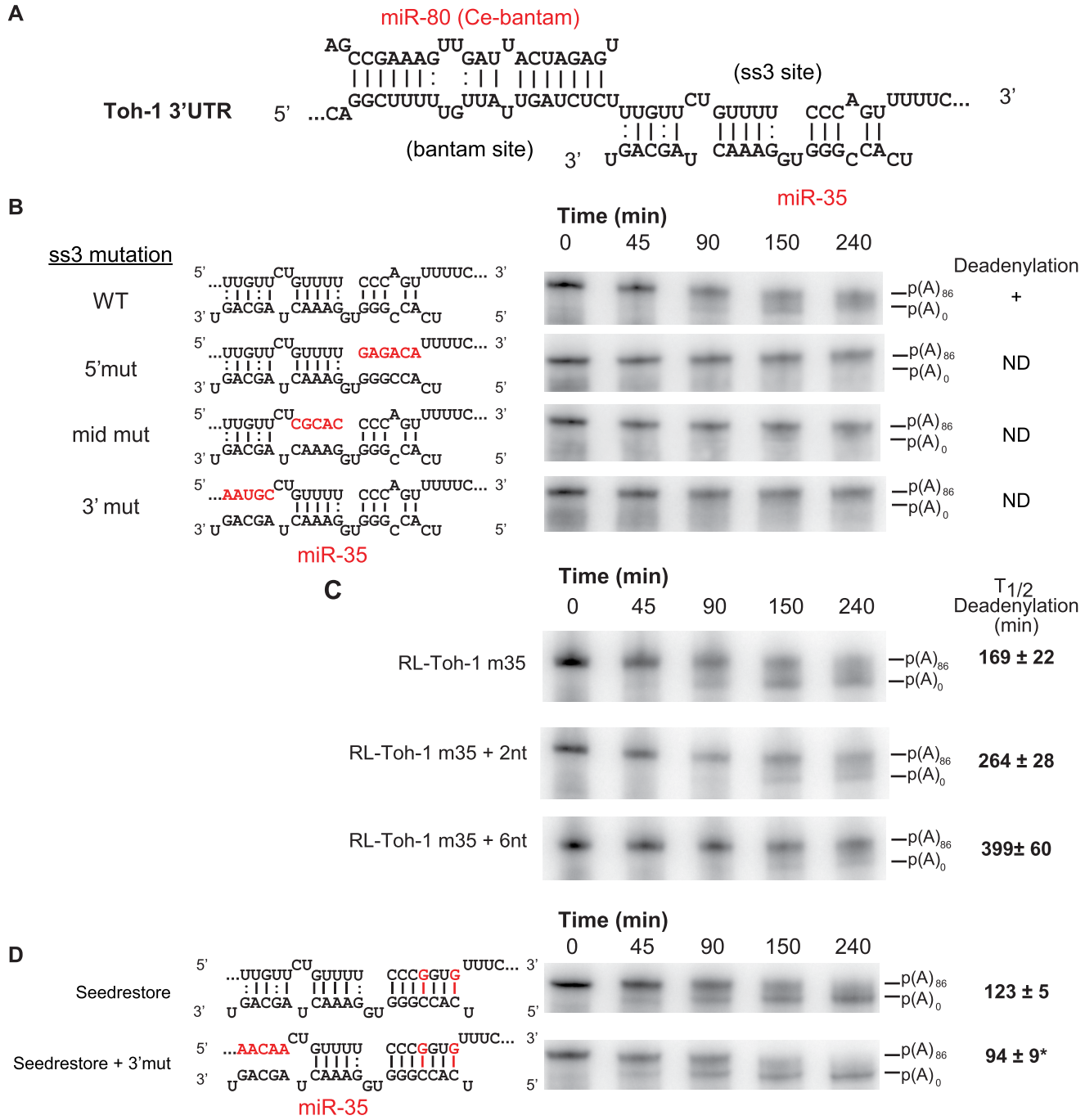

Figure 2. Structural requirements of the ss3 seedless miRNA-binding site. (**A**) Details of the base pairing with the miR-80 and miR-35 (ss3) pair of sites. Only the best-pairing paralog of the Bantam and miR-35-42 families are presented. Watson-Crick (-), and G:U wobble base-pairs (:) are indicated. (**B**) Base pairing requirements for ss3 function. Mutations (indicated in red) in the 5′, mid and 3′ base pairing regions of the seedless site were introduced, and mutant m35 3′UTRs were subjected to deadenylation time-courses. ND: no deadenylation detected. (**C**) Proximity of the Bantam and seedless sites is required for cooperative miRNA-mediated deadenylation. Two and six-nucleotide linkers were introduced between the Bantam and seedless (ss3) miRNA-binding sites, and the resulting 3′UTRs were tested in deadenylation time-courses. Half-completion deadenylation times (T1/2d) for triplicate experiments are indicated on the right. (**D**) Requirements for the 3′ base pairing is different in cooperative seed-seed pairs. Mutant m35 3′UTRs were subjected to deadenylation time courses. Half-completion deadenylation times for triplicate experiments are indicated on the right. (*) denotes a statistically significance in a one sided Welch *T*-test at a *P*-value of <0.05. See also Supplementary Figure S2.

To determine if the cooperative configuration of the Bantam-ss3 site pair of the *toh-1* m35 3′UTR isoform is transposable to other miRNAs, we converted ss3 into a miR-72-binding site. Based on library sequencing (37), miR-72 is abundant in *C. elegans* embryo, although to a lesser extent than the miR-35-42 family. Introduction of a seedless miR-72-pairing site in this context, designed based on the positioning of base-paired nucleotides of ss3, successfully instigated target mRNA deadenylation, although more slowly than WT m35 UTR isoform (Supplementary Figure S2). Conversion into a seed-pairing site potentiated deadenylation, with no significant effect of duplex formation on the 3′-most nucleotides of miR-72 or of enriching G:U wobble base-pairing (Supplementary Figure S2). Overall, these data show that certain configurations of seedless sites allow cooperation with seed-pairing sites in driving target deadenylation and silencing, and that close proximity permits cooperation between a seedless and a seed-pairing site or between two seed-pairing sites. These results further indicate that the potency of seedless miRNA-binding sites and/or their base-pairing requirements in cooperation may be miRNA-specific.

Cooperative recruitment of miRISC to a non-canonical miRNA-binding site

To investigate the interactions involved in this cooperative configuration of miRNA-binding sites, we used biotinylated 2′-*O*-Me oligonucleotides that mimic a single site or pairs of sites encoded in the m35 3′UTR isoform as pulldown baits (24). Various biotinylated 2′-*O*-Me oligonucleotides were incubated in embryonic extracts, pulled down using streptavidin beads, and miRISC capture was probed by western blotting against the miRNA-dedicated Argonautes ALG-1 and ALG-2 and the GW182 homologs AIN-1 and AIN-2 (Figure 3A, Supplementary Figure S3). A single bulged site matching the miR-35–42 family or the *toh-1* Bantam site efficiently captured embryonic miRISC, while a non-specific bait matching human miR-16 did not (Figure 3A). Strikingly, a biotinylated mimic encoding the seedless miR-35 ss3 site failed to capture miRISC on its own (*toh-1* ss3 lane compared to miR-35 lane). This observation raises the possibility that miRISC occupation of the neighbouring seed-pairing Bantam site is required to recruit the miRISC to the additional ss3 site (Figure 3A, upper panel). To test this hypothesis, we examined miRISC capture using baits mimicking the m35 3′UTR pair of sites or baits where each site was individually mutated (Figure 3A, double site pulldown lanes). A bait encoding the cooperating m35 Bantam and ss3 sites was more efficient than a single Bantam site in miRISC capture (Bantam +ss3 lane). Mutation of the ss3 site in the pair of cooperating sites resulted in a reduction in miRISC capture by the remaining Bantam site (Bantam +ss3 mut lane), indicating that ss3 contributes to recruiting miRISC in the double site bait. When the Bantam site was incapacitated while leaving ss3 intact, no miRISC could be captured, again indicating that ss3 cannot recruit miRISC on its own (Bantam mut + ss3 lane). Finally, restoring the seed-pairing sequence of ss3 enhanced miRISC capture far beyond any of the single or double site baits. Displacement of miRISC from individual sites using competitor DNA oligonucleotides, or quantitation using near-infrared detection, led to similar results (Supplementary Figure S3). Recruitment of the miR-35 miRNA to the ss3 site was further confirmed by qRT-PCR (Supplementary Figure S3, see also Materials and Methods), and this interaction was lost upon mutation of either the Bantam or ss3 sites in the bait. Overall, our data demonstrate that the ss3 seedless site is incapable of recruiting miRISC on its own, but proximity to the neighboring seed-pairing site facilitates the cooper-

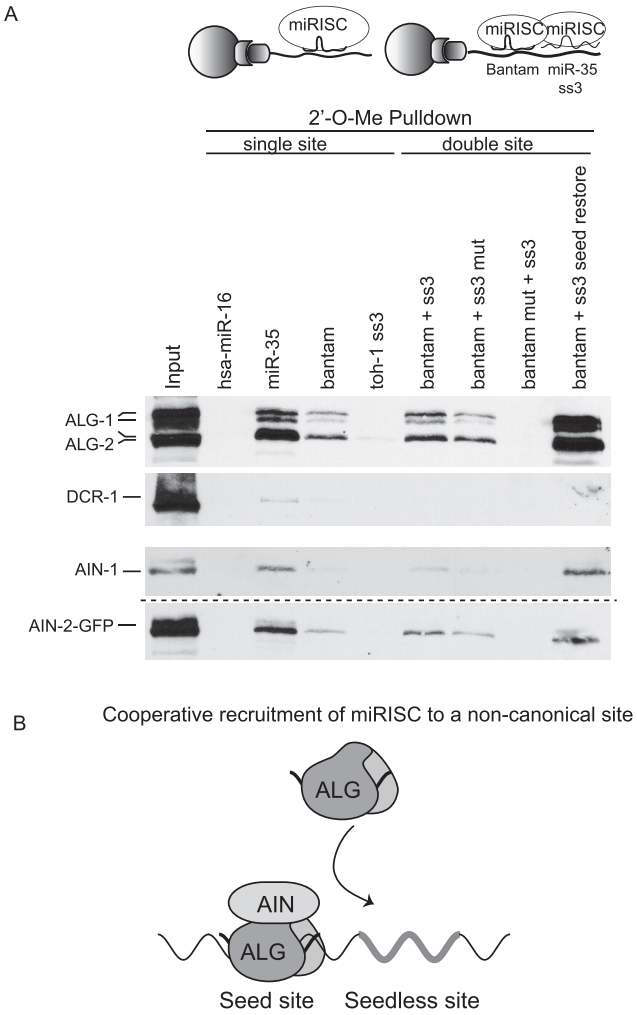

Figure 3. Cooperation of seed-pairing and seedless miRNA-binding sites in recruitment of miRISC. (**A**) Biotinylated 2′-*O*-Me oligonucleotides were used as mimics of single, or double target sites of *toh-1* m35 3′UTR and utilized in miRISC pulldown assays in embryonic extract. Single miRNA-binding site mimics include, from left to right: hsa-miR-16 (negative control), miR-35, Bantam, m35 miR-35 seedless site (ss3 mimic). Cooperating (double) miRNA-binding site mimics include: m35 Bantam + ss3, Bantam + impaired (mut) ss3, impaired (mut) Bantam + ss3, and Bantam + ss3 with its seed restored. Pulled-down miRISC components ALG-1/2, AIN-1 and DCR-1 were analyzed by western blot. Note that data presented in the lowest panel was generated using the *ain-2:gfp* transgenic strain in a distinct pulldown experiment (dotted line). (**B**) Seedless and seed-pairing sites cooperate in miRISC recruitment to the mRNA target. ss3 is required for m35 3′UTR deadenylation but cannot recruit miRISC on its own, and relies on neighboring Bantam site for recruitment. See also Supplementary Figure 3.

ative miRISC recruitment to the seedless site and triggers miRNA-mediated deadenylation (Figure 3B).

Cooperation between miRNA-binding sites is required to recruit Ccr4-Not and for silencing in the *C. elegans* embryo

The properties of Bantam/ss3 pair of sites highlights the importance of cooperative interactions for the recruitment of miRISC to target mRNAs, but how these interactions trigger deadenylation or potentiate silencing is unknown. We recently showed that recruitment of the Ccr4–Not complex to miRNA-binding sites occurs subsequent to the binding of miRISC components ALG-2 and AIN-1 (29). To determine if cooperative interactions are required to recruit Ccr4–Not to target mRNAs, we performed Deadenylated RNA ImmunoPrecipitation (DRIP) (29) assays on reporter mRNAs encoding increasing copies of miRNA-binding sites (Figure 4A–C). For this, strains expressing 3xFLAG tagged versions of ALG-2 and NTL-1 were engineered by editing their endogenous genomic loci with CRISPR–Cas9 (Supplementary Figure S4), and cell-free embryonic extracts were derived (24). Capped, polyadenylated RL mRNAs encoding 0, 1, 3 or 6 miR-35-binding sites were incubated in extracts for 2 h, ALG-2 (miRISC) and NTL-1 (Ccr4-Not) were immunoprecipitated through their 3xFLAG tag, and interacting reporter mRNAs were quantified by qRT-PCR. A single miRNA-binding site was sufficient for ALG-2 to bind to reporter mRNAs, and binding increased significantly with 3 and 6 miR-35-binding sites (Figure 4B). While no significant NTL-1 interaction with mRNA reporters could be detected with a single miR-35-binding site, 3 or 6 binding sites enabled interaction with NTL-1 (Figure 4C). Taken together, these results indicate that the recruitment of the Ccr4–Not complex requires cooperative miRISC interactions on multiple miRNA-binding sites (24). We note, however, that this specific design does not allow a clear distinction between additive and cooperative binding of miRISC to seed-pairing sites.

To determine the importance of cooperative mechanisms for miRNA-mediated silencing *in vivo*, we designed an assay based on the activity of endogenous embryonic miRNAs on an edited endogenous mRNA locus. Loss-of-function mutations in *sel-1* genetically suppress the lethality of the temperature-sensitive *glp-1(e2142)* allele in the *Notch/Delta* cascade (Figure 5A) (38,39). Using CRISPR-Cas9, we engineered strains encoding *sel-1* loci bearing 1, 2 or 3 binding sites within their 3′UTRs for the abundant embryonic miR-35–42 miRNA family. Suppression of the temperature-sensitive *glp-1(e2142)* allele at its non-permissive temperature was thus made to depend upon miRISC activity (Figure 5B and Supplementary Figure S5). Mutant *glp-1(e2142); sel-13′UTR* variant animals were grown at permissive (16°C) or non-permissive (21°C) temperature, and live progeny were counted (Figure 5C and D). A single miR-35-binding site embedded within the *sel-1* 3′UTR did not suppress *glp-1(e2142)* lethality at either temperature (0× versus 1×). However, strains wherein 2 or 3 miR-35-binding sites where embedded within the *sel-1* 3′UTR significantly suppressed *glp-1(e2142)* embryonic lethality at both 16°C (Figure 5C) and 21°C (Figure 5D). We conclude that, as observed *in vitro*, cooperativity between miRNA binding sites is required for silencing *in vivo* in an embryonic context.

A predicted miRISC–miRISC cooperative interface is required for miRNA function *in vivo*

We recently published a computational method to model three-dimensional (3D) structural conformations of target-bound miRISC (30). Using this method, we modeled the possible conformations of the two Argonaute proteins bound to the cooperative Bantam/miR-35 target site pair from the *toh-1* 3′UTR (Figure 6A). We first generated a homology model of the *C. elegans* ALG-2 protein structure based on the crystal structures of the conserved *hs*Ago1 and *hs*Ago2, which share 67% sequence identity with ALG-2 (Supplementary Figure S6). The *hs*Ago2/ALG-2 overlap has an RMSD of 1.5 Å, whereas a similar modeling of ALG-1 produced a less accurate model (∼3 Å); hence we performed all subsequent modeling using ALG-2, which shares ∼86% sequence identity with ALG-1 overall and 94% identity within the MID/PIWI domains (Supplementary Figure S6). We then modeled the RNA duplex structures of miR-80 (a Bantam family miRNA) and miR-35 with their cognate *toh-1* binding sites using the MC-Sym algorithm (31). Each duplex was docked in ALG-2 in an 'open' conformation obtained through an elastic network model that simulates relative motions of the lobes in the protein structure that have some flexibility. Favorable complexes with minor steric clashes were then refined using energy minimization (30). Next, the two bound miRISC units were merged by modeling the possible conformations of CUU linkers connecting the two sites, based on ∼2000 observed single-stranded CUU fragments in the PDB database. We selected and energy minimized conformations of the merged miRISCs with the fewest steric clashes. These favorable complexes fall into two structural groups: structures with and without ALG-2/ALG-2 interactions. For structures without ALG-2 interactions, we found only a couple of single conformations with severely bent CUU linkers. For structures with ALG-2 interactions, we found a cluster of (five or more) closely related conformations with the linkers adopting the typical conformation in a helix. Due to their common occurrence, we chose members of this structural group for subsequent analysis. These models can accommodate two miRISCs in close proximity on the same 3′UTR (Figure 6B) and reveal a distinct RNA-dependent interface between the cooperating Argonautes. In the modeled configuration, an entire surface of the miR-35-bound miRISC (downstream on the mRNA sequence) is closely juxtaposed with the (upstream) miR-80-bound miRISC. The interface is formed by peripheral residues of the PIWI/MID domain that are in close proximity between the two Argonautes and appear to interact through two putative helices (E513-D530 and F726-M742 in ALG-2; E607-D623 and F820-M836 in ALG-1) and nearby loop residues (Figure 6C).

To test the hypothesis that this putative interface constitutes a functional determinant for cooperative miRISC–miRISC interactions, we computationally identified permutations of conserved residues that would be expected to

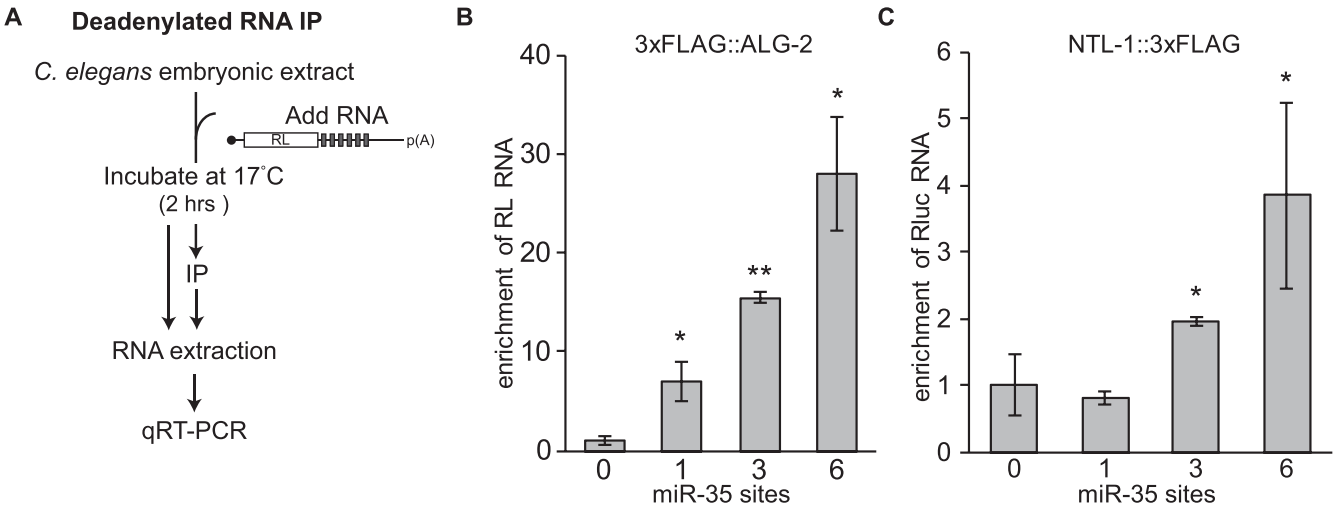

Figure 4. Cooperative recruitment of miRISC and effector machinery. (**A**) Flow chart of the procedure for the modified Deadenylated RNA Immuno Precipitation (DRIP) assay. (**B**) RL mRNAs encoding 0, 1, 3 or 6 miR-35 binding sites were used for DRIP assay in extract prepared from 3xFLAG:ALG-2 (B) or NTL-1:3xFLAG (**C**) embryo. Enrichment of RL RNA bound to 3xFLAG fusions in DRIP relative to the input was determined by qRT-PCR. Error bars represent SD. (*) and (**) denotes statistically significance in a one sided Welch *T*-test at a *P*-value of <0.05 and <0.01 respectively, $n = 3$. See also Supplementary Figure S4.

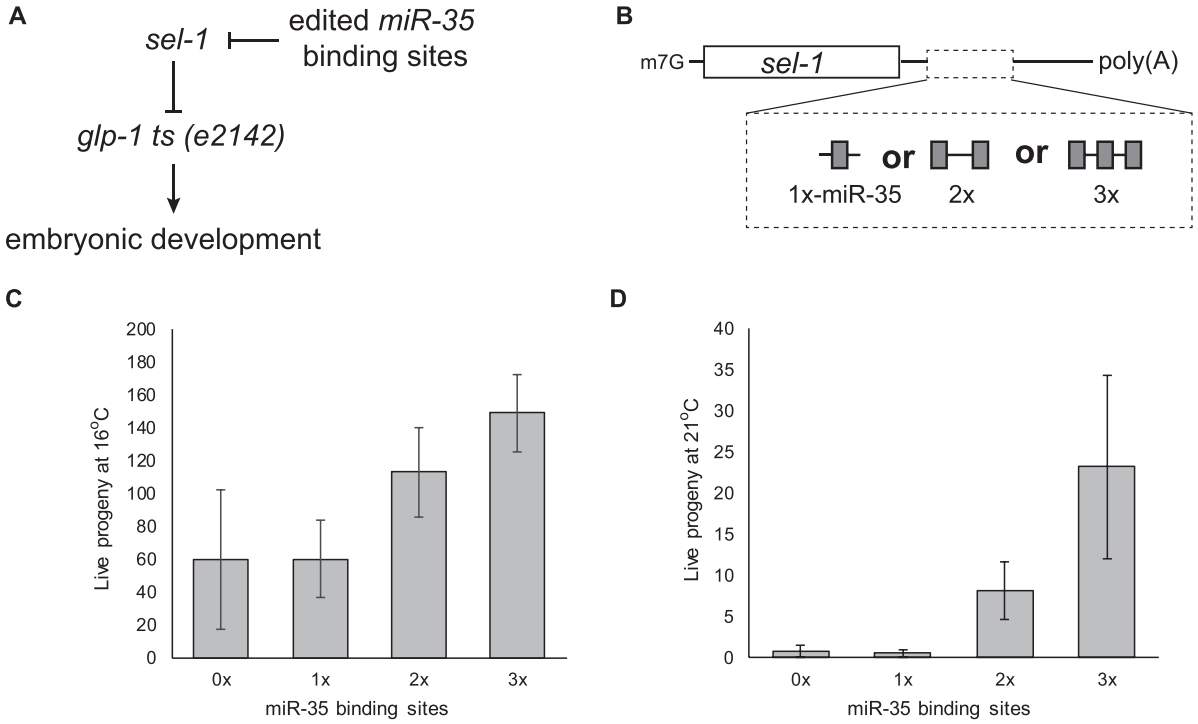

Figure 5. miRNA cooperation is required for silencing *in vivo*. (**A**) *sel-1* loss-of-function genetically suppresses the temperature-sensitive *glp-1(e2142)* allele in the notch/delta cascade. (**B**) Using CRISPR–Cas9, we engineered the *sel-1* endogenous locus to encode 1 (*qe15*), 2 (*qe14*) or 3 (*qe13*) binding sites for the miR-35–42 family of miRNAs. The ability of the edited *sel-1* loci to suppress the temperature-sensitive *glp-1(e2142)* allele is thus made to depend upon miRISC cooperativity. *sel-1* mutant alleles were crossed with the *glp-1(e2142)* allele and live progeny was quantified at 16°C **(C)** and 21°C (**D**). See also Supplementary Figure S5.

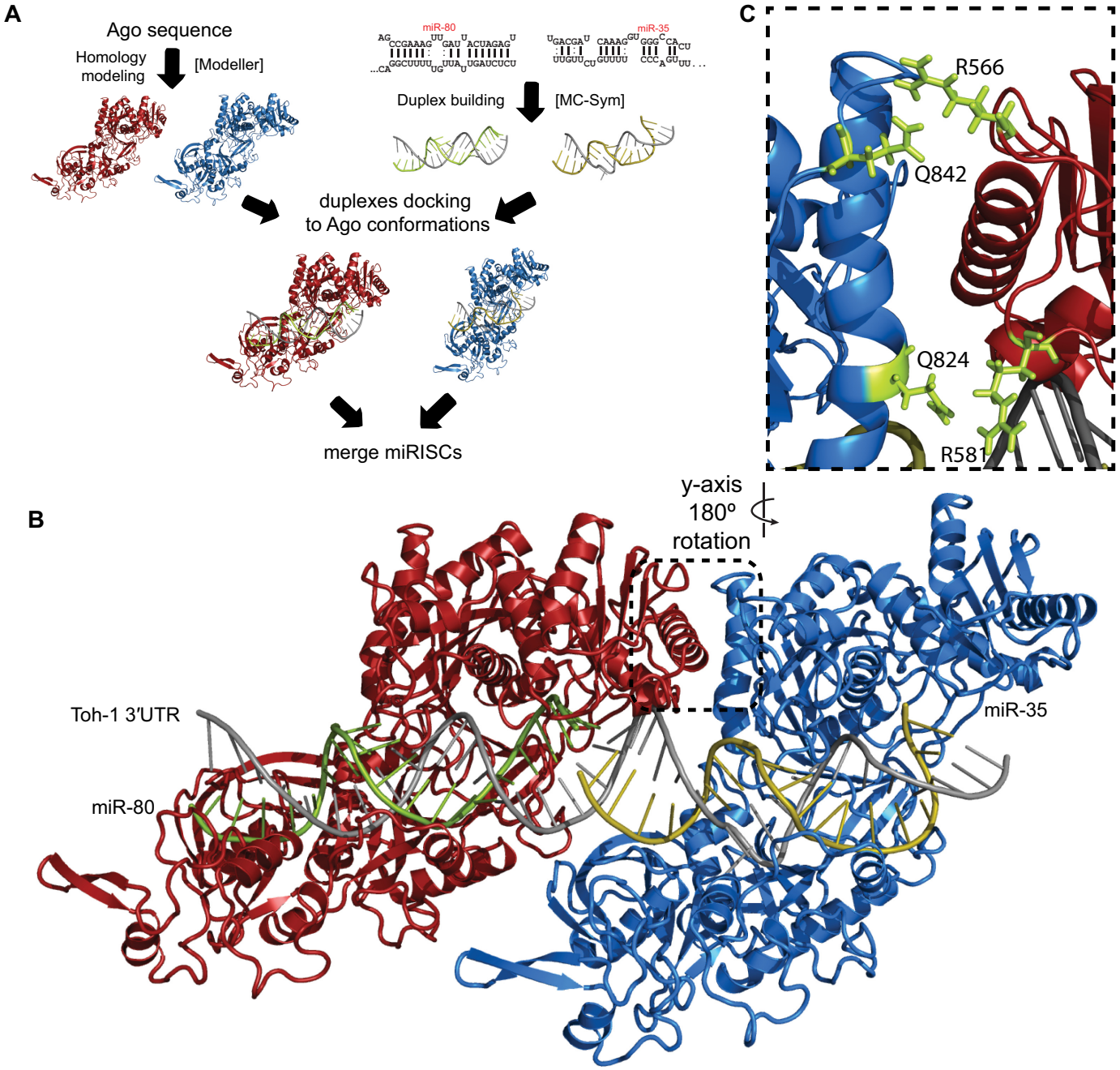

Figure 6. A computational model of miRISC identifies putative cooperative determinants at the interface between Argonaute proteins. (**A**) The miRISC–miRISC structural model was constructed in several steps: homology modeling of ALG-2, building miRNA–target duplexes, docking duplexes to open ALG-2 conformations, and the merging of two miRISC structures by sampling linker conformations (see details in Methods section). (**B**) Model of co-operating miRISCs with miR-80 and miR-35 duplexes on the *toh-1* 3′UTR cooperative binding sites. The dashed box outlines the proposed cooperative interface. (**C**) Cooperative interface showing the two alpha helices in close proximity, as well as the mutated residues in ALG-1 in green. See also Supplementary Figure 6.

impinge on their interactions (Supplementary Figure S6). Our exhaustive computational screen of point mutations focused on residues located in or near the two interfacing helices in the models. We identified the following four mutations producing the most significant changes in Argonaute–Argonaute binding affinity *in silico*: R487N and R471K in the upstream ALG-2 and Q730I and Q748K in the downstream ALG-2. Genetically, *alg-1* and *alg-2* partially compensate for each other, but only *alg-1* null alleles exhibit low penetrance of the gross embryonic or larval phenotypes associated with miRNAs (40,41). We reasoned that mutations in *alg-1* would be more informative about the role of the cooperative determinant residues in miRNA function *in vivo*. We thus engineered the corresponding mutations in *alg-1* using CRISPR-Cas9 genome editing, resulting in variants

R581N, R566K, Q824I and Q842K of ALG-1 (Figure 6B and C).

Three strains harboring the engineered variants—R581N, Q824I and Q842K—displayed a lower brood size (Supplementary Figure S7), and were associated with vulval bursting at the L4-to-adult transitions (Figure 7A), a telltale phenotype for defects in the repressive functions of let-7 on *lin-41* (42). Whereas this phenotype is rare in WT (N2) animals (<1%), the engineered ALG-1 cooperative interface variants exacerbated bursting at 25°C (6.0, 2.4 and 3.3%, for R581N, Q824I and Q842K, respectively). Compounding mutations with *alg-2(ok304)* significantly exacerbated the penetrance of this phenotype, especially for the R581N variant (27.1, 5.5 and 4.0% bursting, respectively). In contrast, the ALG-1(R566K) variant did not lead to any significant effect under the same conditions.

To examine the physiological significance of the putative cooperative interface for the function of miRNAs in a different context, we tested the engineered mutations for genetic interactions with a hypomorphic *lsy-6* allele. The lsy-6 miRNA determines the left/right asymmetry of ASEL and ASER neurons during embryogenesis by targeting *cog-1,* a suppressor of ASEL fate (43). The *cog-1* mRNA encodes several target sites for embryonic miRNAs, two of which are recognized by the lsy-6 miRNA. The *lsy-6(ot150)* hypomorphic allele results in reduced lsy-6 expression and a partial, temperature sensitive, loss of ASEL. The resulting defects can be tracked using *plim-6*::*GFP*, a transcriptional reporter that serves as an indicator for successful *cog-1* silencing by lsy-6 miRNA. This sensitized miRNA functional assay has been extensively used to look at genetic interactions with the miRNA pathway (28,44–46). For example, a null allele of *alg-1* results in loss of ASEL in about 50% of *lsy-6(ot150)* individuals at the permissive temperature (20°C), compared to 15–20% in the *alg-1(wt)* background (45). In contrast, null *alg-2* alleles do not appreciably affect ASEL determination (Supplementary Figure S7), indicating that repression of *cog-1* by *lsy-6* is mainly mediated through *alg-1*. Interestingly, strains encoding the R581N, Q842K, and Q824I variants of ALG-1 exhibited 38, 42 and 34% loss of ASEL at 25°C, respectively (Figure 7B), whereas the R566K variant did not affect the incidence of ASEL fate. These results indicate that residues R581, Q842 and Q824 of ALG-1 are required for lsy-6-directed silencing of *cog-1*.

The four tested residues were identified on the basis of their location and contacts in a modeled miRISC/miRISC cooperative interface. To understand the mechanistic implications of the putative interfacing residues on miRISC function, we first tested their importance for miRISC protein–protein interactions and for target site recognition. miRISC capture using miR-35 and Bantam 2′-*O*-Me target site analogs were carried out on embryonic lysates derived from *alg-2(ok304)* animals and double mutants expressing the ALG-1 variants Q842K, Q824I and R566K (Figure 7C). No major difference in expression or miRISC capture could be observed with phenocritical ALG-1 variants. Furthermore, miR-35 expression levels were not reduced in the variant genotypes (Supplementary Figure S7). miRISC capture carried out on young adult lysates using let-7 baits led to similar results (Figure 7D, Supplementary Figure S7). Although we cannot account for minor differences with these techniques, these results indicate that ALG-1 variants retained their proficiency in maturing miRNAs and in finding cognate targets.

Interfacing residues are located in the vicinity of but do not overlap with the tryptophan pocket of ALG-1, the conserved GW182-binding determinant (Supplementary Figure S6). As such, the investigated variants are not expected to directly impact on AIN-1 binding. ALG-1 variants were immunoprecipitated from embryonic lysates, and interaction with the GW182 homolog AIN-1 was monitored by western blotting. Interactions of R566K, R581N and Q842K with AIN-1 were indistinguishable from WT(N2) in this assay. Unexpectedly, Q824I impaired ALG-1 co-immunoprecipitation with AIN-1 (Supplementary Figure S7), and impinged on recovery of AIN-1 in miRISC captures (Figure 7C), suggesting that this residue indirectly participates in the interaction with AIN-1 or is involved in its stabilization in the miRISC complex. Together, these results demonstrate that although the R581 and Q842 residues are required for miRNA function *in vivo,* they do not substantially affect the *individual* functions and interactions of miRISC *in vitro*. The effect of Q824I on AIN-1 interaction, and the proximity of this residue with R581 and Q842, nonetheless support a model wherein the influence that the cooperative miRISC–miRISC interactions exert on the effector Ccr4–Not complex is conveyed through the AIN-1 miRISC scaffold (Figure 7E, see also Discussion). To begin testing this model, we derived extracts from embryos expressing the ALG-1(R581N) variant in the *alg-2(ok304)* null background and examined its deadenylase activity on a 3xmiR-35 reporter. Deadenylation driven by the ALG-1(R581N) variant was slower than in the control extract (Figure 7F). We conclude that residues and contacts implicated in the modeled miRISC–miRISC interface are involved in the cooperative recruitment and/or activation of the miRISC effector complex.

DISCUSSION

Prediction algorithms often portray mRNAs as targets for multiple miRNAs, sometimes dozens, often clustered in contiguous portions of 3′UTRs. When considering the additional regulatory layers intertwined in the sequences and structures of 3′UTRs, the possibility of functional and mechanistic interplay – both positive and negative – between mRNAs, miRISC and RNA-binding proteins appears unavoidable. In line with earlier genomic surveys, our previous study in a *C. elegans* embryonic cell-free system responsive to natural 3′UTR sequences hinted at the cooperative contribution of miRNA-binding sites in target deadenylation. The molecular basis for their cooperation, however, remained elusive. Here, the properties of a non-canonical miRNA-binding site in a 3′UTR isoform were instrumental in uncovering multiple mechanisms of miRNA cooperation.

An allosteric model for miRNA-mediated silencing

Our results substantiate and untangle two distinct cooperative mechanisms. First, target-bound miRISC favors additional Argonaute protein recruitment. This mechanism is

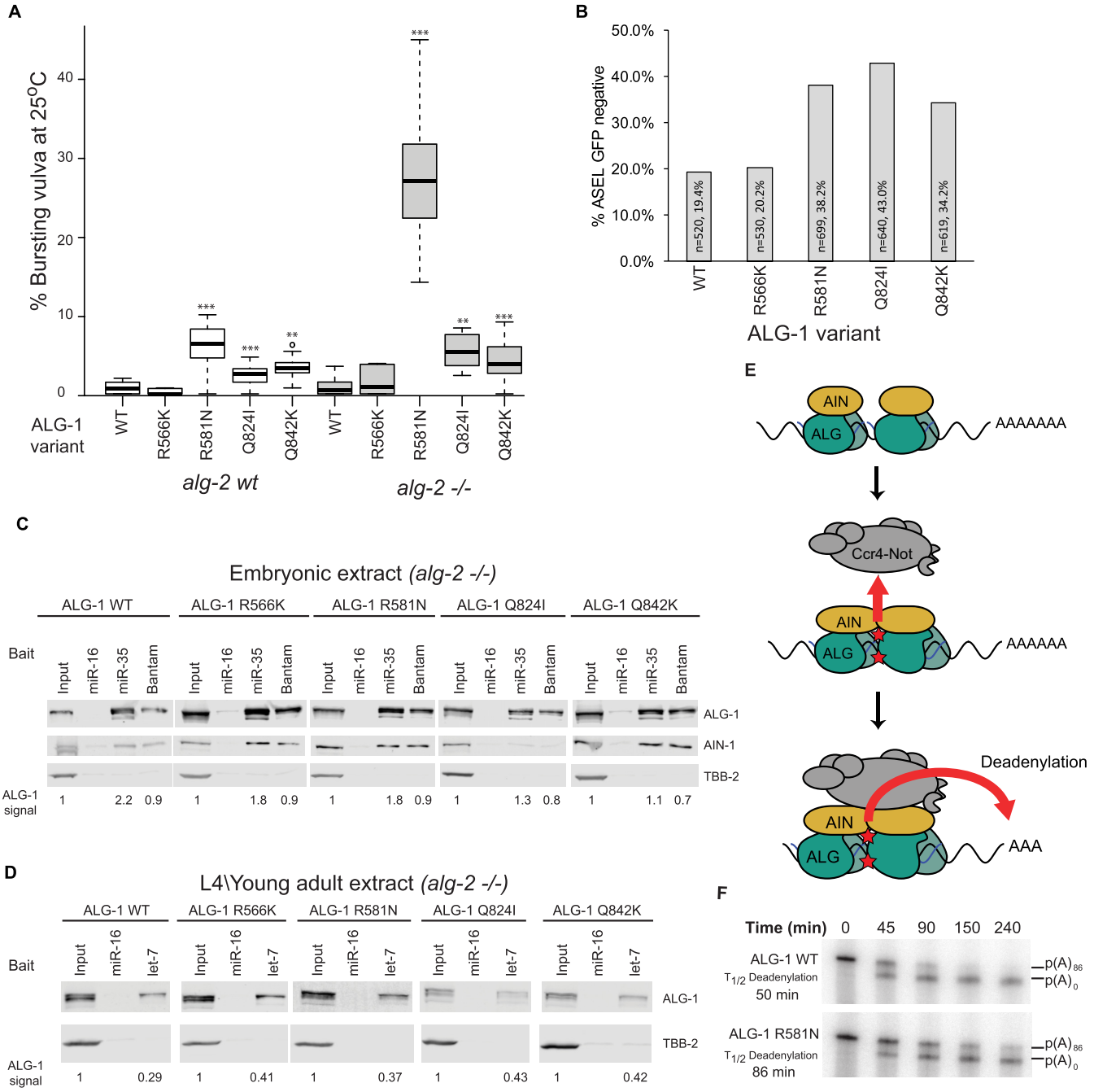

Figure 7. Mutations in the putative Argonaute cooperative interface result in miRNA defects *in vivo*. (**A**) Bursting vulva was quantified for strains expressing the indicated engineered ALG-1 variants in *WT* or *alg-2(ok304)* (–/–) backgrounds. Experiments were carried out at 25°C. $n = 10$, $^{**}P < 0.01$, $^{***}P < 0.001$ on a Welch's two-sided *T*-test compared to WT. (**B**) Alleles encoding ALG-1 variants genetically interact with lsy-6. Engineered alleles were crossed with OH3646 (*otIs114(Plim-6::GFP, rol-6);lsy-6(ot150)*. Animals were scored for GFP in the ASEL neuron. Experiments were carried out at 25°C. (**C**) 2′-*O*-Me pulldowns analysis of variant ALG-1 miRISC from embryonic lysates using 5′-biotinylated 2′-*O*-Me oligos encoding hsa-miR-16 (non-cognate), miR-35 and Bantam binding sites. Quantitative western blot for ALG-1, AIN-1 and TBB-2 were performed using near infrared fluorescent antibody. The ratio of the pulldown fraction against input is indicated below. (**D**) 2′-*O*-Me pulldowns analysis of variant ALG-1 miRISCs from young adult lysates using hsa-miR-16 and let-7 binding site baits. ALG-1 and TBB-2 were analyzed by quantitative western blot. Experiments in (C) and (D) were performed in the *alg-2(ok304)* genotype. (**E**) An allosteric model of miRNA-mediated silencing. Upon binding of multiple miRISC, contacts within the Argonaute-Argonaute interface trigger allosteric structural changes (red stars) in Argonaute and AIN proteins, which enable the recruitment and activation of the Ccr4–Not1 deadenylase complex. (**F**) Radiolabelled RL-3×miR35-p(A)$_{86}$ was subjected to an *in vitro* deadenylation assay in *alg-2(ok304)* and *alg-2(ok304);alg-1(R581N)* extracts. RNA was extracted and analyzed by UREA-PAGE and autoradiography. See also Supplementary Figure S7.

essential for the recruitment of miRISC to at least a subset of non-canonical sites, which cannot recruit the complex on their own. It is conceivable that target binding enables Argonaute–Argonaute contacts that favor the cooperative recruitment of additional miRISC to additional miRNA-binding sites. Such an interaction should be distinct from a steady state, or static dimer; interaction of a loaded Argonaute with a first target site must alter its structure to favor interactions with other miRISC units. Although our design did not specifically address the importance of these interactions among seed-binding sites, it had already been supported by prior work using mammalian cell reporters (23).

Second, we show that target site cooperation is necessary for the recruitment and/or stabilization of the Ccr4–Not effector complex to target mRNAs. For this to happen a signal must be conveyed from the cooperative binding sites to the Argonaute–Argonaute interface, and in turn to AIN-1 in order to license the recruitment of the Ccr4–Not effector complex. However, we cannot assume that the recruitment of Ccr4–Not to a physiological target mRNA is sufficient to trigger its deadenylation, nor should we expect that different miRNA-binding site configurations drive the same degree of translational repression, mRNA deadenylation, and decay. As such, an additional and distinct mechanism may involve the allosteric *activation* of one or more of the activities associated with the Ccr4–Not effector complex (Figure 7E). Common to all three postulated mechanisms are changes in Argonaute structure driven by cooperative miRNA-binding sites, which result in the regulation of allosteric interactions. We propose that the contacts or structural changes that involve the conserved R581 and Q842 residues of ALG-1 participate in one or more of those cooperative mechanisms.

Other non-mutually exclusive models remain plausible to explain miRNA cooperativity. For example, cooperativity may also involve structural changes to AIN-1, or to the target mRNA within or around the interacting sites. Furthermore, and although two distinct mechanisms of cooperativity are essential for the properties of the Bantam/ss3 pair of sites, cooperativity in binding may not always be required for cooperativity in effector recruitment or activation. Some cooperative site configurations may exploit only one of these mechanisms, a combination, and possibly new ones.

Several recent publications have highlighted the flexible and dynamic nature of the Argonaute structure (30,47–49). The outlined allosteric model provides a conceptual framework to explain how this inherent property of Argonautes can play a crucial part in its interactions and functions. This model also contrasts with prior models that featured static and stoichiometric interactions between the miRNA, its target, the Argonaute, GW182 proteins and the Ccr4–Not effector. Part of those differences likely stem from the limits of early approaches in the resolution of miRISC dynamics. Assays such as the tethering of miRISC proteins to reporter mRNAs and interaction assays using recombinant fragments, however insightful to identify important interactions and functions, may have contributed to this oversight. The emerging quantitative single-molecule imaging methods will likely contribute to further disambiguate the stoichiometry and the dynamic nature of miRISC and its Ccr4-Not effector assemblies *in situ*.

A role for non-canonical binding sites in cooperative miRNA-mediated silencing

Recent publications support both the frequent incidence and the functional importance of non-canonical miRNA-binding sites in transcriptomes (17,50,51). The cooperative seed-pairing/seedless configuration presented here suggests that at least a subset of non-canonical sites participates in cooperative mechanisms of miRISC recruitment and/or in potentiation of silencing. Because of the degenerate nature of miRNAs outside the seed, it is likely that critical determinants of non-canonical sites will be specific to individual miRNAs/target sites. Additional factors such as the number of non-canonical miRNA-binding sites that can be simultaneously involved, or the directionality of their configurations, remain to be explored. Until those requirements are defined, the prediction of non-canonical sites will remain a challenge and their prevalence will remain unclear. Furthermore, distinct modes of non-canonical pairing may lead to qualitatively different outcomes. For example, a recent publication showed that extensive 3′ pairing of miRNAs involved in non-canonical binding sites could lead to their de-stabilization *in vitro* (52).

The current work indicates that some of the principles underlying non-canonical target sites may only be appreciable in the context of the target-bound miRISC. For example, the important contribution of 3′ base-pairing in non-canonical sites (50) evokes a role for the PAZ domain of the Argonaute, which binds the 3′ sequence of miRNAs (53). The interactions of this domain with the miRNA are profoundly reorganized as a consequence of 3′ base pairing (54). 3D modeling using the methods exploited here can shed light on the structural constraints within miRISC and on the determinants that enable distinctive base-pairing conformations. Detailing the binding kinetics of individual and cooperating binding sites could validate the predicted structural models and contribute to further resolution of the intrinsic movements that underlie miRISC functions. The recent identification of functional differences between miRNA paralogs on canonical sites, dictated by nucleotides outside the seed, suggest that such an approach could be fruitful with seed-pairing sites as well (16).

On the prevalence of miRNA cooperativity

The results of our *in vitro* and *in vivo* assays support a strong contribution for cooperative mechanisms in miRNA-mediated silencing in the *C. elegans* embryo and larval stages. Cell-free deadenylation in embryonic lysates and *in vivo sel-1/glp-1* suppression assays suggest that, at least in some contexts, cooperativity may be strictly required for miRNA function. Although the presence of multiple nearby sites is not proof of cooperativity, many important *C. elegans* miRNA targets feature multiple functional binding sites. Seven sites for lin-4 were linked to *lin-14* regulation, several of which non-canonical (55,56), *lin-28* is regulated by nearby lin-4 and let-7 sites (57,58), *lin-41* mRNA encodes two functional let-7 sites (42,57), and *cog-1* 3′UTR

bears two functional lsy-6 sites that may also function cooperatively (59). In spite of this apparent prevalence, miRNA cooperativity is clearly not an evolutionary specialization of miRNA-mediated silencing in *C. elegans*. Cooperativity had been noticed early on with artificial reporters in mammalian cultured cells (60) and in several genome-wide surveys of the output of miRNA-binding sites (21).

Furthermore, cooperativity may not be necessary for miRNA function in all contexts and several mechanisms can be envisioned to modulate its importance. For example, miRISC subunits and co-factors can be expressed or associated differentially in a cellular or tissue-specific manner. Alternatively, one of the many conserved phosphorylation sites on Argonautes that have recently been identified (61) (M.J. Simard, *personal communication*) may instigate the allosteric changes necessary to recruit the effector complex. Animal development requires extreme spatio-temporal control of gene expression. A consequence of a strictly cooperative action of miRNAs is that it precisely limits their activity to a window wherein multiple miRNAs and their targets are associated with a coordinated stoichiometry. In contrast, a fully differentiated tissue may not require such fine-tuning. The identification of conserved cooperative determinants in this study will enable a perspective of the breadth of the cooperative functions of miRNAs across cells and species.

In outlook, the cooperative mechanisms substantiated in this paper will likely extend much beyond miRISC-to-miRISC interactions, and influence the combinatorial regulation of mRNAs more generally. A growing number of examples of functional cooperation have been reported wherein RNA-binding proteins can enhance miRNA functions (46,62,63). Genomic insight into the location and frequency of binding sites for RNA-binding proteins is rapidly expanding through *in vivo* cross-linking methods for RNA-binding proteins coupled with next-generation sequencing. Such methods hold great promise in capturing the complexity of the interplay between regulatory sequences encoded in 3′UTRs.

SUPPLEMENTARY DATA

Supplementary Data are available at NAR Online.

ACKNOWLEDGEMENTS

We apologize to authors whose relevant work may not have been cited in this manuscript. We would like to thank Martin J. Simard for providing ALG-1, AIN-1 and AIN-2 antibodies, and the High Performance Computing at NYU Abu Dhabi.

Author contributions: All authors contributed to project design. M.N.F. performed all wet lab experiments, with a contribution of V.M. to Figure 7. H.H.G. performed *in silico* modeling and computational screening for ALG variants. M.N.F. and T.F.D. wrote the manuscript with assistance from co-authors.

FUNDING

Some strains were provided by the CGC, which is funded by NIH Office of Research Infrastructure Programs [P40 OD010440]; Canadian Institute of Health Research (CIHR) [MOP 123352 to T.F.D.]; Canada Foundation for Innovation (CFI); Fonds de la Recherche en Santé du Québec, Chercheur-Boursier Senior salary award (to T.F.D.); Mathieu Flamand was the recipient of the CIHR Vanier Doctoral Research Award; National Institutes of Health [NHGRI U01 HG004276, to K.C.G.]; NYU Abu Dhabi. Funding for open access charge: CIHR [MOP 123352].

Conflict of interest statement. None declared.

REFERENCES

1. Ambros,V. (2004) The functions of animal microRNAs. *Nature*, **431**, 350–355.
2. Bartel,D.P. (2009) MicroRNAs: target recognition and regulatory functions. *Cell*, **136**, 215–233.
3. Fabian,M.R., Sonenberg,N. and Filipowicz,W. (2010) Regulation of mRNA translation and stability by microRNAs. *Annu. Rev. Biochem.*, **79**, 351–379.
4. Kim,V.N., Han,J. and Siomi,M.C. (2009) Biogenesis of small RNAs in animals. *Nat. Rev. Mol. Cell. Biol.*, **10**, 126–139.
5. Krol,J., Loedige,I. and Filipowicz,W. (2010) The widespread regulation of microRNA biogenesis, function and decay. *Nat. Rev. Genet.*, **11**, 597–610.
6. Fabian,M.R. and Sonenberg,N. (2012) The mechanics of miRNA-mediated gene silencing: a look under the hood of miRISC. *Nat. Struct. Mol. Biol.*, **19**, 586–593.
7. Giraldez,A.J., Mishima,Y., Rihel,J., Grocock,R.J., Van Dongen,S., Inoue,K., Enright,A.J. and Schier,A.F. (2006) Zebrafish MiR-430 promotes deadenylation and clearance of maternal mRNAs. *Science*, **312**, 75–79.
8. Baek,D., Villen,J., Shin,C., Camargo,F.D., Gygi,S.P. and Bartel,D.P. (2008) The impact of microRNAs on protein output. *Nature*, **455**, 64–71.
9. Fabian,M.R., Mathonnet,G., Sundermeier,T., Mathys,H., Zipprich,J.T., Svitkin,Y.V., Rivas,F., Jinek,M., Wohlschlegel,J., Doudna,J.A. *et al.* (2009) Mammalian miRNA RISC recruits CAF1 and PABP to affect PABP-dependent deadenylation. *Mol. Cell*, **35**, 868–880.
10. Behm-Ansmant,I., Rehwinkel,J., Doerks,T., Stark,A., Bork,P. and Izaurralde,E. (2006) mRNA degradation by miRNAs and GW182 requires both CCR4:NOT deadenylase and DCP1:DCP2 decapping complexes. *Genes Dev.*, **20**, 1885–1898.
11. Eulalio,A., Huntzinger,E., Nishihara,T., Rehwinkel,J., Fauser,M. and Izaurralde,E. (2009) Deadenylation is a widespread effect of miRNA regulation. *RNA*, **15**, 21–32.
12. Bazzini,A.A., Lee,M.T. and Giraldez,A.J. (2012) Ribosome profiling shows that miR-430 reduces translation before causing mRNA decay in zebrafish. *Science*, **336**, 233–237.
13. Lewis,B.P., Burge,C.B. and Bartel,D.P. (2005) Conserved seed pairing, often flanked by adenosines, indicates that thousands of human genes are microRNA targets. *Cell*, **120**, 15–20.
14. Vella,M.C., Choi,E.Y., Lin,S.Y., Reinert,K. and Slack,F.J. (2004) The C. elegans microRNA let-7 binds to imperfect let-7 complementary sites from the lin-41 3′UTR. *Genes Dev.*, **18**, 132–137.
15. Didiano,D. and Hobert,O. (2006) Perfect seed pairing is not a generally reliable predictor for miRNA-target interactions. *Nat. Struct. Mol. Biol.*, **13**, 849–851.
16. Wolter,J.M., Le,H.H., Linse,A., Godlove,V.A., Nguyen,T.D., Kotagama,K., Lynch,A., Rawls,A. and Mangone,M. (2016) Evolutionary patterns of metazoan microRNAs reveal targeting principles in the let-7 and miR-10 families. *Genome Res.*, **1**, 53–63.
17. Broughton,J.P., Lovci,M.T., Huang,J.L., Yeo,G.W. and Pasquinelli,A.E. (2016) Pairing beyond the seed supports MicroRNA targeting specificity. *Mol. Cell*, **64**, 320–333.
18. Chi,S.W., Hannon,G.J. and Darnell,R.B. (2012) An alternative mode of microRNA target recognition. *Nat. Struct. Mol. Biol.*, **19**, 321–327.
19. Shin,C., Nam,J.W., Farh,K.K., Chiang,H.R., Shkumatava,A. and Bartel,D.P. (2010) Expanding the microRNA targeting code: functional sites with centered pairing. *Mol. Cell*, **38**, 789–802.

20. Lal,A., Navarro,F., Maher,C.A., Maliszewski,L.E., Yan,N., O'Day,E., Chowdhury,D., Dykxhoorn,D.M., Tsai,P., Hofmann,O. *et al.* (2009) miR-24 Inhibits cell proliferation by targeting E2F2, MYC, and other cell-cycle genes via binding to "seedless" 3′UTR microRNA recognition elements. *Mol. Cell*, **35**, 610–625.
21. Grimson,A., Farh,K.K., Johnston,W.K., Garrett-Engele,P., Lim,L.P. and Bartel,D.P. (2007) MicroRNA targeting specificity in mammals: determinants beyond seed pairing. *Mol. Cell*, **27**, 91–105.
22. Saetrom,P., Heale,B.S., Snove,O. Jr, Aagaard,L., Alluin,J. and Rossi,J.J. (2007) Distance constraints between microRNA target sites dictate efficacy and cooperativity. *Nucleic Acids Res.*, **35**, 2333–2342.
23. Broderick,J.A., Salomon,W.E., Ryder,S.P., Aronin,N. and Zamore,P.D. (2011) Argonaute protein identity and pairing geometry determine cooperativity in mammalian RNA silencing. *RNA*, **17**, 1858–1869.
24. Wu,E., Thivierge,C., Flamand,M., Mathonnet,G., Vashisht,A.A., Wohlschlegel,J., Fabian,M.R., Sonenberg,N. and Duchaine,T.F. (2010) Pervasive and cooperative deadenylation of 3′UTRs by embryonic microRNA families. *Mol. Cell*, **40**, 558–570.
25. Brenner,S. (1974) The genetics of Caenorhabditis elegans. *Genetics*, **77**, 71–94.
26. Ward,J.D. (2015) Rapid and precise engineering of the Caenorhabditis elegans genome with lethal mutation co-conversion and inactivation of NHEJ repair. *Genetics*, **199**, 363–377.
27. Paix,A., Folkmann,A., Rasoloson,D. and Seydoux,G. (2015) High efficiency, homology-directed genome editing in Caenorhabditis elegans using CRISPR-Cas9 ribonucleoprotein complexes. *Genetics*, **201**, 47–54.
28. Flamand,M.N., Wu,E., Vashisht,A., Jannot,G., Keiper,B.D., Simard,M.J., Wohlschlegel,J. and Duchaine,T.F. (2016) Poly(A)-binding proteins are required for microRNA-mediated silencing and to promote target deadenylation in C. elegans. *Nucleic Acids Res.*, **44**, 5924–5935.
29. Wu,E., Vashisht,A.A., Chapat,C., Flamand,M.N., Cohen,E., Sarov,M., Tabach,Y., Sonenberg,N., Wohlschlegel,J. and Duchaine,T.F. (2016) A continuum of mRNP complexes in embryonic microRNA-mediated silencing. *Nucleic Acids Res.* ,**4** , 2081 -2098 .
30. Gan,H.H. and Gunsalus,K.C. (2015) Assembly and analysis of eukaryotic Argonaute-RNA complexes in microRNA-target recognition. *Nucleic Acids Res.*, **43**, 9613–9625.
31. Parisien,M. and Major,F. (2008) The MC-Fold and MC-Sym pipeline infers RNA structure from sequence data. *Nature*, **452**, 51–55.
32. Gan,H.H. and Gunsalus,K.C. (2013) Tertiary structure-based analysis of microRNA-target interactions. *RNA*, **19**, 539–551.
33. Mangone,M., Manoharan,A.P., Thierry-Mieg,D., Thierry-Mieg,J., Han,T., Mackowiak,S.D., Mis,E., Zegar,C., Gutwein,M.R., Khivansara,V. *et al.* (2010) The landscape of C. elegans 3′UTRs. *Science*, **329**, 432–435.
34. Jan,C.H., Friedman,R.C., Ruby,J.G. and Bartel,D.P. (2011) Formation, regulation and evolution of Caenorhabditis elegans 3′UTRs. *Nature*, **469**, 97–101.
35. Hutvagner,G., Simard,M.J., Mello,C.C. and Zamore,P.D. (2004) Sequence-specific inhibition of small RNA function. *PLoS Biol.*, **2**, E98.
36. Kruger,J. and Rehmsmeier,M. (2006) RNAhybrid: microRNA target prediction easy, fast and flexible. *Nucleic Acids Res.*, **34**, W451–W454.
37. Stoeckius,M., Maaskola,J., Colombo,T., Rahn,H.P., Friedlander,M.R., Li,N., Chen,W., Piano,F. and Rajewsky,N. (2009) Large-scale sorting of C. elegans embryos reveals the dynamics of small RNA expression. *Nat. Methods*, **6**, 745–751.
38. Priess,J.R., Schnabel,H. and Schnabel,R. (1987) The glp-1 locus and cellular interactions in early C. elegans embryos. *Cell*, **51**, 601–611.
39. Kodoyianni,V., Maine,E.M. and Kimble,J. (1992) Molecular basis of loss-of-function mutations in the glp-1 gene of Caenorhabditis elegans. *Mol. Biol. Cell*, **3**, 1199–1213.
40. Grishok,A., Pasquinelli,A.E., Conte,D., Li,N., Parrish,S., Ha,I., Baillie,D.L., Fire,A., Ruvkun,G. and Mello,C.C. (2001) Genes and mechanisms related to RNA interference regulate expression of the small temporal RNAs that control C. elegans developmental timing. *Cell*, **106**, 23–34.
41. Vasquez-Rifo,A., Jannot,G., Armisen,J., Labouesse,M., Bukhari,S.I., Rondeau,E.L., Miska,E.A. and Simard,M.J. (2012) Developmental characterization of the microRNA-specific C. elegans Argonautes alg-1 and alg-2. *PLoS One*, **7**, e33750.
42. Ecsedi,M., Rausch,M. and Grosshans,H. (2015) The let-7 microRNA directs vulval development through a single target. *Dev. Cell*, **32**, 335–344.
43. Johnston,R.J. and Hobert,O. (2003) A microRNA controlling left/right neuronal asymmetry in Caenorhabditis elegans. *Nature*, **426**, 845–849.
44. Bosse,G.D., Ruegger,S., Ow,M.C., Vasquez-Rifo,A., Rondeau,E.L., Ambros,V.R., Grosshans,H. and Simard,M.J. (2013) The decapping scavenger enzyme DCS-1 controls microRNA levels in Caenorhabditis elegans. *Mol. Cell*, **50**, 281–287.
45. Zinovyeva,A.Y., Bouasker,S., Simard,M.J., Hammell,C.M. and Ambros,V. (2014) Mutations in conserved residues of the C. elegans microRNA Argonaute ALG-1 identify separable functions in ALG-1 miRISC loading and target repression. *PLoS Genet.*, **10**, e1004286.
46. Hammell,C.M., Lubin,I., Boag,P.R., Blackwell,T.K. and Ambros,V. (2009) nhl-2 Modulates microRNA activity in Caenorhabditis elegans. *Cell*, **136**, 926–938.
47. Chandradoss,S.D., Schirle,N.T., Szczepaniak,M., MacRae,I.J. and Joo,C. (2015) A dynamic search process underlies microRNA targeting. *Cell*, **162**, 96–107.
48. Wang,Y., Juranek,S., Li,H., Sheng,G., Tuschl,T. and Patel,D.J. (2008) Structure of an argonaute silencing complex with a seed-containing guide DNA and target RNA duplex. *Nature*, **456**, 921–926.
49. Wang,Y., Juranek,S., Li,H., Sheng,G., Wardle,G.S., Tuschl,T. and Patel,D.J. (2009) Nucleation, propagation and cleavage of target RNAs in Ago silencing complexes. *Nature*, **461**, 754–761.
50. Loeb,G.B., Khan,A.A., Canner,D., Hiatt,J.B., Shendure,J., Darnell,R.B., Leslie,C.S. and Rudensky,A.Y. (2012) Transcriptome-wide miR-155 binding map reveals widespread noncanonical microRNA targeting. *Mol. Cell*, **48**, 760–770.
51. Zisoulis,D.G., Lovci,M.T., Wilbert,M.L., Hutt,K.R., Liang,T.Y., Pasquinelli,A.E. and Yeo,G.W. (2010) Comprehensive discovery of endogenous Argonaute binding sites in Caenorhabditis elegans. *Nat. Struct. Mol. Biol.*, **17**, 173–179.
52. Park,J.H., Shin,S.Y. and Shin,C. (2017) Non-canonical targets destabilize microRNAs in human Argonautes. *Nucleic Acids Res.*, **45**, 1569–1583.
53. Song,J.J., Liu,J., Tolia,N.H., Schneiderman,J., Smith,S.K., Martienssen,R.A., Hannon,G.J. and Joshua-Tor,L. (2003) The crystal structure of the Argonaute2 PAZ domain reveals an RNA binding motif in RNAi effector complexes. *Nat. Struct. Biol.*, **10**, 1026–1032.
54. De,N., Young,L., Lau,P.W., Meisner,N.C., Morrissey,D.V. and MacRae,I.J. (2013) Highly complementary target RNAs promote release of guide RNAs from human Argonaute2. *Mol. Cell*, **50**, 344–355.
55. Lee,R.C., Feinbaum,R.L. and Ambros,V. (1993) The C. elegans heterochronic gene lin-4 encodes small RNAs with antisense complementarity to lin-14. *Cell*, **75**, 843–854.
56. Wightman,B., Ha,I. and Ruvkun,G. (1993) Posttranscriptional regulation of the heterochronic gene lin-14 by lin-4 mediates temporal pattern formation in C. elegans. *Cell*, **75**, 855–862.
57. Reinhart,B.J., Slack,F.J., Basson,M., Pasquinelli,A.E., Bettinger,J.C., Rougvie,A.E., Horvitz,H.R. and Ruvkun,G. (2000) The 21-nucleotide let-7 RNA regulates developmental timing in Caenorhabditis elegans. *Nature*, **403**, 901–906.
58. Moss,E.G., Lee,R.C. and Ambros,V. (1997) The cold shock domain protein LIN-28 controls developmental timing in C. elegans and is regulated by the lin-4 RNA. *Cell*, **88**, 637–646.
59. Didiano,D. and Hobert,O. (2008) Molecular architecture of a miRNA-regulated 3′ UTR. *RNA*, **14**, 1297–1317.
60. Doench,J.G. and Sharp,P.A. (2004) Specificity of microRNA target selection in translational repression. *Genes Dev.*, **18**, 504–511.
61. Lopez-Orozco,J., Pare,J.M., Holme,A.L., Chaulk,S.G., Fahlman,R.P. and Hobman,T.C. (2015) Functional analyses of phosphorylation events in human Argonaute 2. *RNA*, **21**, 2030–2038.
62. Jing,Q., Huang,S., Guth,S., Zarubin,T., Motoyama,A., Chen,J., Di Padova,F., Lin,S.C., Gram,H. and Han,J. (2005) Involvement of microRNA in AU-rich element-mediated mRNA instability. *Cell*, **120**, 623–634.
63. Nolde,M.J., Saka,N., Reinert,K.L. and Slack,F.J. (2007) The Caenorhabditis elegans pumilio homolog, puf-9, is required for the 3′UTR-mediated repression of the let-7 microRNA target gene, hbl-1. *Dev. Biol.*, **305**, 551–563.